A method for the estimate of broadband directionnal surface albedo from a geostationary satellite

Bernard Pinty, Ramond D.

A Method for the Estimate of Broadband Directional Surface Albedo from a Geostationary Satellite

B. PINTY AND D. RAMOND

L.A.M.P./O.P.G.C., Université de Clermont II, 63170 Aubière, France

(Manuscript received 3 April 1987, in final form 12 June 1987)

ABSTRACT

Surface albedo can be inferred from geostationary satellite measurements as long as the effects due to the atmosphere, the spectral response of the sensor, and the angular anisotropy of the reflected field are corrected. In this paper, we developed a method which includes ad hoc correction procedures for the three categories of effects. An application of the method is conducted over the Sahara and the African Sahel using METEOSAT radiances together with auxiliary data derived from other satellites (Tiros-N and Nimbus-7) and standard meteorological observations. The surface albedo maps are estimated over this region, at a spatial resolution compatible with one used in climate models, for 2 days representative of the dry and the wet seasons, respectively. The observed seasonal surface albedo change and the relationships between the surface and the planetary albedos are discussed in order to examine the validity of the method and the correction procedures.

1. Introduction

The ability of existing climate models to parameterize reasonable short time-scale fluctuations such as diurnal variations at the surface as well as to assess the impact of climate change on the biosphere partly depends on future improvements in modeling land surface processes. Achievement of these improvements necessitates, at the grid scale of climate models ($1° \times 1°$ or $2° \times 2°$), the development of parameterizations of mass and energy exchanges between the surface and the atmosphere and simultaneously, it requires a good knowledge and appropriate description of surface properties at the same scale.

Among the concerned set of surface properties, the albedo was inventoried, almost 10 years ago, as being an important parameter of the biosphere (Charney, 1975). Several numerical investigations (e.g., Otterman, 1974; Berkofsky, 1976; Charney et al., 1977; Sud and Fenessy, 1982) clearly support the idea of a link between surface albedo variations and significant perturbations of atmospheric dynamic processes induced through feedback mechanisms. After reviewing sensitivity studies of climate models to surface albedo changes, Henderson-Sellers and Wilson (1983) have recommended an accuracy of ± 0.05 in surface albedo for climate modeling purposes. This recommendation raises the difficult question of whether surface albedo mapping can be achieved with the proposed accuracy from existing data. Satellite-borne instruments constitute a unique tool for obtaining and monitoring surface albedo on the global scale at a spatial resolution adequate for climate modeling. In turn, the above assertion implies that the problems hindering a quantitative estimate of surface albedo by increasing the uncertainty of this estimate must be examined.

In order to infer broadband surface albedo from a single observation made at the top of the atmosphere by a narrowband sensing instrument, one has to know or assume (i) the angular distribution of the reflected energy to get hemispherical reflectance or albedo; (ii) the conversion factor which must be applied to filtered radiances to derive broadband radiances; and (iii) the optical state and properties of the intervening atmosphere to correct for its masking effect. The assessment of these three points requires a priori knowledge of the state of the sensed medium (e.g., type of surface cover, characteristics and distribution of the aerosols) and its physical properties in relation with the solar electromagnetic radiation (e.g., through surface bidirectional or atmospheric models). Some of these requirements concern physical behaviors which are still poorly documented and scarcely observed even at a local scale. Moreover, these requirements constitute drastic constraints with regard to the potentiality and the objectives of satellite measurements. Because of the lack of congruent auxiliary information, it is necessary to use existing data routinely delivered by surface conventional networks, and several operational satellites in order to derive a simplified but still acceptable and realistic method.

It is our main concern through this paper to propose such a method for inferring surface albedo over western Africa, a sensitive climatic region including the Sahara Desert and part of the African Sahel. Owing to the geographical location of the studied region, the European METEOSAT satellites provide a major database. In the proposed method, the first step is to estimate a

reference albedo value over a site located in the studied region, instrumented with routine meteorological measurements; the complete surface albedo mapping is achieved in a second step with the help of an additional assumption on the field of atmospheric transmittances. A brief summary of the results from previous studies of the three previously mentioned categories of effects is given in section 2. The proposed method is described in section 3. The data selected for its application over western Africa are presented in section 4 and the results are analyzed in section 5. Finally a discussion of the correction procedures we used is given in section 6.

2. Summary of previous results

a. Angular anisotropy of the reflected field

The knowledge of the bidirectional reflection properties of the sensed medium is a prerequisite for inferring flux quantities such as albedo from a single angle observation made by a narrow field of view instrument. Using data from the Nimbus-7 Earth Radiation Budget (ERB) experiment, Taylor and Stowe (1984) have documented the anisotropic behavior of the optical properties of "land" and "desert" regions over the total solar range. Among extensive informations about the non-Lambertian properties of these surfaces, a significant azimuthal anisotropy is observed from the Nimbus-7 dataset even for small solar and satellite zenith angles. Due to the relative course of the sun during the year, this anisotropy can induce a systematic bias in the estimate of seasonal albedo changes over intertropical regions studied with METEOSAT or other geostationary satellites.

A suitable way to take these reflection properties into account has been recently proposed by Pinty and Ramond (1986). Indeed, using photometric relationships designed for lunar and Martian regions (Minnaert, 1941; Hapke, 1963; Kieffer et al., 1977) together with the anisotropic factors deduced from Nimbus-7 ERB experiment, these authors have derived an analytical expression describing the bidirectional reflectance $\rho(\theta_0, \theta_v, \psi)$ and the albedo $a(\theta_0)$ for two broad categories of terrestrial surfaces, namely "land" and "desert":

$$\rho(\theta_0, \theta_v, \psi) = \rho_0 f_r \tag{1}$$

$$a(\theta_0) = \rho_0 f_a \tag{2}$$

with

$$f_r = \cos^{k-1}(\theta_0)\cos^{k-1}(\theta_v)[1 + (1-k^2)\cos^2(\zeta)]$$

$$f_a = 2\frac{\cos^{k-1}(\theta_0)}{k+1}\left\{1 + \frac{(1-k^2)}{k+3}[k\cos^2(\theta_0) + 1]\right\}$$

$$\cos(\zeta) = \cos(\theta_0)\cos(\theta_v) + \sin(\theta_0)\sin(\theta_v)\cos(\psi),$$

where θ_0 and θ_v are the solar zenith angle and the satellite viewing angle respectively; ψ is the relative azimuth between the two optical paths; ζ the phase angle; the parameter k indicates the level of anisotropy of the sensed medium—the values derived by Pinty and Ramond are 0.84 for land regions and 0.94 for desert regions. In the previous expression, the main unknown is the surface reflectance value at overhead sun and nadir observation ρ_0; once this value is determined and the surface type is identified, then the bidirectional reflectance as well as the hemispherical reflectance are directly available.

b. Spectral sampling by the METEOSAT visible channel

The retrieval of broadband (0.3–3 μm) radiances L_{SOL} from filtered radiances L_{SAT} measured by METEOSAT visible channel requires the knowledge of the appropriate conversion factor F_{SOL}:

$$L_{SOL} = F_{SOL} L_{SAT} \tag{3}$$

with

$$L_{SAT} = \int_{0.3}^{3\,\mu m} L_{T\lambda}\tau_{SAT\lambda}\, d\lambda$$

$$L_{SOL} = \int_{0.3}^{3\,\mu m} L_{T\lambda}\, d\lambda,$$

where $L_{T\lambda}$ is the spectral radiance leaving the top of the atmosphere and $\tau_{SAT\lambda}$ the spectral response of the METEOSAT visible channel.

The F_{SOL} factor depends on the relative distribution of the radiances over the shortwave solar range with respect to the spectral response of the METEOSAT sensor. As a consequence, the conversion factor behavior is driven by the observational geometry parameters, the atmospheric radiative state and the optical properties of the surface. For instance, Koepke (1983) has shown that the conversion factor may vary between 2.8 ± 1 and 2.4 ± 1 for vegetated and bare surfaces, respectively. In order to reduce the uncertainty due to this factor in the albedo estimate, it is necessary to account for its spatial and temporal variations, specially when studying a large climatic region where a wide range of surface cover type exists.

Using a theoretical approach, Stum et al. (1985) have established a parameterized expression which allows a first estimate of METEOSAT conversion factors from the major optically acting parameters which can be known on a routine basis. This expression is given as a function of the relative observational geometry; two atmospheric parameters; the surface visibility and the water vapor content; and two surface parameters, the broadband albedo and the spectral band ratio built around the 0.7 μm wavelength which is analogous to the vegetation index available from AVHRR data. Although this parameterized expression of the conversion factor uses rough representation of atmospheric and surface properties, it has the advantage of simplicity to

provide a first level of correction for the METEOSAT filter function.

c. Masking effect of the atmosphere

The atmosphere intervenes through a transmittance factor along the double path defined by the relative position of the sun, the surface and the satellite, and also by the addition of its intrinsic radiance. In a recent paper, Pinty and Szejwach (1985) have proposed a ratio technique in order to remove the masking effects of the atmosphere over whole climatic regions where detailed knowledge of the atmospheric properties is not achievable; this technique is based on the realistic assumption that, for cloudless conditions, the atmospheric transmittance has a characteristic spatial scale greater than the grid scale which is relevant for climatological studies of the surface albedo (typically 100–200 km) (Bouka Biona and Boutin, 1985). It follows that the spatial variations of the radiances emerging at the top of the atmosphere between neighboring sites can be related to the spatial variations of their surface reflectances. In practice, the reflectance ratios between neighboring sites are simply derived from a linear regression between their respective radiances measured during a diurnal cycle by a geostationary satellite.

The absolute reflectance values are obtained from these ratios by using a reference value determined in a first step over one of the sites where simultaneous measurements of radiances at the top of the atmosphere and surface global radiation are available (Pinty et al., 1985; Pinty and Tanré, 1987).

3. Method description

The present method uses the ratio technique described by Pinty and Szejwach (1985) for removing the atmospheric effects and it includes the above recalled correction procedures to account for the selective spectral response of the sensor and the anisotropy of the reflected field.

a. First step: Reference albedo estimate

In the approach we develop here, the basic equation for the spectral radiance at the top of a cloud free atmosphere (Justus and Paris, 1985) is given by

$$\pi L_{T\lambda}(\theta_0,\theta_v,\psi)=\pi L_{a\lambda}(\theta_0,\theta_v,\psi)+E_{0\lambda}\cos(\theta_0)[\rho_\lambda(\theta_0,\theta_v,\psi)T_{d\lambda}(\theta_0)+a_\lambda(\theta_0)E_\lambda(\theta_0)][T_{d\lambda}(\theta_v)+E_\lambda(\theta_v)]. \quad (4)$$

In (4), $L_{a\lambda}$ denotes the upwelling sky radiance, $E_{0\lambda}$ the terrestrial solar irradiance, $T_{d\lambda}$ and E_λ the direct beam and diffuse atmospheric transmittances, respectively; ρ_λ is the bidirectional reflectance of the surface and a_λ the hemispherical reflectance. For sake of simplicity, the minor contribution of higher order scattering between the surface and the atmosphere has been neglected. In order to emphasize the surface anisotropic contribution, (4) can also be written as follows:

$$\pi L_{T\lambda}(\theta_0,\theta_v,\psi)=\pi L_{a\lambda}(\theta_0,\theta_v,\psi)+E_{0\lambda}\cos(\theta_0)\{\rho_\lambda(\theta_0,\theta_v,\psi)T_\lambda(\theta_0)T_\lambda(\theta_v)+[a_\lambda(\theta_0)-\rho_\lambda(\theta_0,\theta_v,\psi)]E_\lambda(\theta_0)T_\lambda(\theta_v)\}, \quad (5)$$

where T_λ is the total (direct + diffuse) transmissivity. When the surface behaves like a Lambertian reflector, the second term in brackets in (5) vanishes and this equation reduces to the usual formulation of the spectral radiance over a Lambertian surface.

By integrating (5) over the spectral range lying between 0.3 and 3 μm (i.e., the whole solar range) and using the mean integral value theorem, we can derive (6) with the introduction of the conversion factor F_{SOL}:

$$\pi F_{SOL}L_{SAT}(\theta_0,\theta_v,\psi)=\pi L_a(\theta_0,\theta_v,\psi)+E_0\cos(\theta_0)\{\rho(\theta_0,\theta_v,\psi)T(\theta_0)a_T+[a(\theta_0)-\rho(\theta_0,\theta_v,\psi)]E(\theta_0)a_{Td}\} \quad (6)$$

with

$$E_0\cos(\theta_0)=\int_{0.3}^{3\,\mu m}E_{0\lambda}\cos(\theta_0)d\lambda,$$

$$\rho(\theta_0,\theta_v,\psi)=\frac{\int_{0.3}^{3\,\mu m}E_{0\lambda}\cos(\theta_0)\rho_\lambda(\theta_0,\theta_v,\psi)d\lambda}{\int_{0.3}^{3\,\mu m}E_{0\lambda}\cos(\theta_0)d\lambda},$$

$$a(\theta_0)-\rho(\theta_0,\theta_v,\psi)=\frac{\int_{0.3}^{3\,\mu m}E_{0\lambda}\cos(\theta_0)[a_\lambda(\theta_0)-\rho_\lambda(\theta_0,\theta_v,\psi)]d\lambda}{\int_{0.3}^{3\,\mu m}E_{0\lambda}\cos(\theta_0)d\lambda},$$

where $T(\theta_0)$ and $E(\theta_0)$ are the total and diffuse incident transmittances over the whole solar spectrum, respectively.

In (6) the a_T and a_{Td} factors are defined as

$$a_T=\frac{T(\theta_0,\theta_v)}{T(\theta_0)}$$

$$a_{Td}=\frac{T_E(\theta_0,\theta_v)}{E(\theta_0)}$$

$$T(\theta_0,\theta_v)=\frac{\int_{0.3}^{3\,\mu m}E_{0\lambda}\cos(\theta_0)\rho_\lambda(\theta_0,\theta_v,\psi)T_\lambda(\theta_0)T_\lambda(\theta_v)d\lambda}{\int_{0.3}^{3\,\mu m}E_{0\lambda}\cos(\theta_0)\rho_\lambda(\theta_0,\theta_v,\psi)d\lambda},$$

$$T(\theta_0)=\frac{\int_{0.3}^{3\,\mu m} E_{0\lambda}\cos(\theta_0)T_\lambda(\theta_0)d\lambda}{\int_{0.3}^{3\,\mu m} E_{0\lambda}\cos(\theta_0)d\lambda}$$

$$T_E(\theta_0,\theta_v)=\frac{\int_{0.3}^{3\,\mu m} E_{0\lambda}\cos(\theta_0)[a_\lambda(\theta_0)-\rho_\lambda(\theta_0,\theta_v,\psi)]E_\lambda(\theta_0)T_\lambda(\theta_v)d\lambda}{\int_{0.3}^{3\,\mu m} E_{0\lambda}\cos(\theta_0)[a_\lambda(\theta_0)-\rho_\lambda(\theta_0,\theta_v,\psi)]d\lambda},$$

$$E(\theta_0)=\frac{\int_{0.3}^{3,\mu m} E_{0\lambda}\cos(\theta_0)E_\lambda(\theta_0)d\lambda}{\int_{0.3}^{3\,\mu m} E_{0\lambda}\cos(\theta_0)d\lambda}.$$

The use of the a_T and a_{Td} factors is convenient for relating the double-way transmittances $T(\theta_0, \theta_v)$ and $T_E(\theta_0, \theta_v)$ to the transmittances $T(\theta_0)$ and $E(\theta_0)$ which can be deduced from ground based measurements such as the global and diffuse radiation. A detailed presentation of the a_T factor and its estimate from routine observations have been given by Pinty and Tanré (1987). Following the same approach, the derivation of the a_{Td} factor is given in the Appendix.

Finally, the introduction of the analytical expression derived by Pinty and Ramond (1986) for $\rho(\theta_0, \theta_v, \psi)$ and $a(\theta_0)$ leads to (7):

$$\pi F_{SOL}L_{SAT}(\theta_0,\theta_v,\psi)=\pi L_a(\theta_0,\theta_v,\psi)+\rho_0 E_0\cos(\theta_0)T(\theta_0)a_T f_r(\theta_0,\theta_v,\psi)\times\left\{1+\left[\frac{f_a}{f_r}-1\right]\frac{rd(\theta_0)a_{Td}}{a_T}\right\}, \quad (7)$$

where $rd(\theta_0)$ designates the ratio of diffuse to global surface radiation.

This approximate expression (Eq. 7) for the radiance at the top of the atmosphere allows a simple estimate of reference ρ_0 values over sites where simultaneous satellite and ground based radiation measurements are available. Table 1 lists the additional parameters which are required for solving (7) and the source of computational procedures. According to Stum et al. (1985), the surface albedo is a decisive parameter for retrieving broadband radiances from the METEOSAT filtered radiances. Since the broadband albedo is a priori unknown, an iterative computational procedure must be applied over the conversion factor F_{SOL} and the surface albedo, in order to get consistent values of these two parameters when convergence is achieved.

b. Second step: Surface albedo mapping

The second step of the ratio technique concerns the estimate of the albedo values over noninstrumented areas corresponding to the greater part of the studied climatic region. In this step the climatic region is meshed so that each grid mesh, hereafter referred to as "site", corresponds to a size area of approximately 100 × 100 km. According to Pinty et al. (1985), since this size area is lesser than the characteristic spatial scale of atmospheric transmittance, the representativeness of the derived averaged albedos depends on the natural heterogeneities of the surface optical properties inside each site.

For two neighboring sites noted "1" and "2", respectively, $T(\theta_0)a_T$ and $L_a(\theta_0, \theta_v, \psi)$ can be related through

$$[T(\theta_0)a_T]_2=[T(\theta_0)a_T]_1+\epsilon Ta_T \quad (8)$$

$$[L_a(\theta_0,\theta_v,\psi)]_2=[L_a(\theta_0,\theta_v,\psi)]_1+\epsilon L_a, \quad (9)$$

where ϵTa_T and ϵL_a are small quantities.

Therefore, the two equations obtained from (7) at sites 1 and 2 can be combined to derive (10):

$$(F_{SOL}L_{SAT})_2=(F_{SOL}L_{SAT})_1 a_c\frac{\rho_{02}}{\rho_{01}}+b_c \quad (10)$$

with

$$a_c\approx\frac{\cos(\theta_0)_2 f_{r2}}{\cos(\theta_0)_1 f_{r1}}\times\left\{1+\left[\frac{f_a}{f_r}-1\right]_2\left[\frac{rda_{Td}}{a_T}\right]_2-\left[\frac{f_a}{f_r}-1\right]_1\left[\frac{rda_{Td}}{a_T}\right]_1\right\},$$

and

$$b_c=\frac{\epsilon L_a}{\pi}+\frac{E_0}{\pi}\cos(\theta_0)_2\rho_{02}f_{r2}\left\{1+\left[\frac{f_a}{f_r}-1\right]_2\left[\frac{rda_{Td}}{a_T}\right]_2\right\}\epsilon Ta_T+\frac{L_{a1}}{\pi}\left[1-\frac{\rho_{02}}{\rho_{01}}\frac{\cos(\theta_0)_2 f_{r2}}{\cos(\theta_0)_1 f_{r1}}\right].$$

TABLE 1. List and estimate procedures of the additional parameters intervening in (7) to derive surface reflectance values at reference sites.

Parameter	Source for the computational procedure	Required data
$L_a(\theta_0, \theta_v, \psi)$	Deschamps et al. (1981)	Visibility, water vapor content
a_T, a_{Td}	Pinty and Tanré (1987)	Visibility, water vapor content, spectral band ratio
f_a, f_r	Pinty and Ramond (1986)	Identification of the surface type (i.e., desert or land region)
F_{SOL}	Stum et al. (1985)	Visibility, water vapor content, spectral band ratio, surface albedo

Considering this expression of a_c (limited to the first order), it appears that the difference between the second and the third terms within brackets remains close to zero if there are no steep changes in the optical state of the atmosphere between the two neighboring sites nor in the anisotropic behavior of their surfaces. Neglect of this difference implies that the significant relative spatial variations of the surface reflectances are only due to the first term which depends upon their bidirectional components. Since the intervening angles are known and if the two surface types are identified (i.e., desert or land region), then the a_c term can be calculated.

The effects due to the spatial variation in the optical state of the atmosphere between the two sites are mainly contained in the b_c term. If the same optical properties prevail over the two sites, the b_c value is close to zero because the only contribution is from the last term. Larger absolute values of the b_c term are obtained when the absorbing properties of the atmosphere due to the aerosols and the atmospheric gases vary between the two sites; for such cases, ϵL_a and $\epsilon T a_T$ are together increased or decreased. An ambiguous situation occurs when the change in the atmospheric properties is only due to a spatial variation in the aerosol optical depth; indeed, this case leads to ϵL_a and $\epsilon T a_T$ having opposite signs, and the balance between the first and the second terms in b_c depends on the surface reflectance value.

Under conditions where the diurnal variation in the b_c term is small (for instance when b_c is close to zero), the ratio ρ_{02}/ρ_{01} can be derived from a linear regression between the radiances $(F_{SOL}L_{SAT})_2$ and $(F_{SOL}L_{SAT})_1 a_c$ which are available from the measurements made by a geostationary satellite during a whole clear sky day over sites 1 and 2. With a similar treatment, the reflectance ratios ρ_{03}/ρ_{02}, ρ_{04}/ρ_{03}, . . . , ρ_{0n}/ρ_{0n-1} can be estimated over successive sites within the climatic region. The absolute reflectance values ρ_{02}, ρ_{03}, . . . , ρ_{0n} are then derived from the knowledge of the reflectance value ρ_0 which has been previously calculated over the reference site with (7). Finally, the ρ_0 values are introduced in (1) and (2) in order to obtain the bidirectional reflectances and the directional albedos. The procedure proposed in the first step of the technique to treat the dependency of the F_{SOL} factor with respect to the surface optical properties is applied in the second step.

4. Data selection and processing

a. *METEOSAT data*

The region selected for application of the ratio technique includes the Sahara Desert and the western part of the African Sahel. Observations on 18 February 1979 and 2 July 1979 have been retained here; in the following, it is assumed that each of these 2 days are, respectively, representative of the dry and wet seasonal conditions which characterize this climatic region. These two dates have been selected after an analysis of the diurnal sequences of infrared METEOSAT pictures from which a large part of West Africa appears cloud free.

In our application, raw data from the METEOSAT visible channel are used to calculate the filtered radiances L_{SAT} at the top of the atmosphere. The spectral response of the visible sensor extends from 0.4 to 1.1 μm and exhibits a quasi-triangular shape with a maximum response at 0.725 μm; the calibration curve derived by Koepke (1982) has been adopted to calculate the L_{SAT} values. In this application, satellite radiances have been spatially averaged over 20 × 20 pixels so that each averaged value corresponds to a size area of approximately 100 × 100 km.

b. *Auxiliary data*

1) FIRST STEP

Over the studied region and for the two selected days, scarcity of surface data limits the retrieval of ρ_0 reference values to three locations in Burkina-Faso: Ouagadougou (12.42°N, 1.5°W), Dori (14.05°N, 0°) and Fada-Ngourma (12.06°N, 0.4°E). The three locations are instrumented with pyranometers operated by the AGRHYMET office which provide surface global radiation measurements. In addition, standard meteorological data such as surface dewpoint and horizontal visibility are routinely available. Following the approach suggested by Reitan (1963), the surface dewpoint is used to estimate the total water vapor content. The coefficients of the empirical relationship have been adjusted monthly using radiosonde data.

The spectral band ratio can be approximated by the normalized vegetation index currently derived from AVHRR data (Tarpley et al., 1984). The same index is also used to identify the surface type by introducing a threshold value of 0.1 for the index. [When the index value is lower (greater) than 0.1, the site is classified in a desert (land) region.]

2) SECOND STEP

A priori knowledge of the surface type is required for the estimate of the a_c term introduced in the second step of the ratio technique. Here again, the normalized vegetation index derived from AVHRR data is used to identify the class to which the different sites belong.

Since the meteorological data required for the F_{SOL} estimate are not available at each site, we have only distinguished the two subregions delimited by the location of the ITCZ (intertropical convergence zone), and we have assumed constant values for the water vapor content over each subregion. The meteorological maps show that the ITCZ oscillates between 8° to 10°N for 18 February and 15° to 16°N for 2 July 1979; from the scattered surface data, values of 1 and 4 cm for the total water vapor content may be expected north and south of the ITCZ location, respectively. Since no sys-

TABLE 2a. Results of the application of the first step of the ratio technique over three reference sites on 18 February 1979.

Test sites	Time (UTC)	$T(\theta_0)_{a_T}$	$\frac{rd(\theta_0)\,a_{Td}}{a_T}$	F_{SOL}	ρ_0	$\rho(\theta_0, \theta_v, \psi)$	$a(\theta_0)$	$a(\theta_0 = 0)$
Ouagadougou	1130	0.612	0.186	2.657	0.189	0.248	0.236	0.235
Dori	1130	0.656	0.186	2.607	0.258	0.339	0.322	0.320
Fada-Ngourma	1130	0.619	0.186	2.660	0.186	0.243	0.232	0.231

tematic variations are observed in the horizontal visibility, a constant value of 20 km corresponding to usual clear sky conditions has been assumed over the whole climatic region.

5. Results

a. *Reference albedos*

The surface reflectances and albedos derived from (7) at the three reference sites are given in Tables 2a and 2b for 18 February and 2 July 1979, respectively. The calculations were made using data obtained near local noon and consequently, the surface albedos calculated with the actual value of the solar zenith angle ($\theta_0 \sim 25°$ for 18 February and $\theta_0 \sim 10°$ for 2 July) are approximately equal to those calculated with hypothetical overhead sun conditions. The bidirectional reflectances derived on 18 February with the actual angles are systematically greater than the surface albedos by about 5% of the mean value at the three studied sites; in the case of 2 July, the difference between these two surface parameters become much closer to zero. Following Pinty and Ramond's (1986) analysis, this change in the anisotropic behavior of the surfaces between the two days is easily explained by the variation in the relative azimuth of the sun and the satellite which is nearly 10° for 18 February and 160° for 2 July at the times of the measurements.

The comparison of the albedo values obtained with hypothetical overhead sun conditions indicates a seasonal decrease in surface albedo which can be quantified by the SV index defined as

$$SV = 100(a_{Jul} - a_{Feb})/a_{Feb}. \qquad (11)$$

The estimated values of SV are −3%, −6% and −10% at the Fada-Ngourma, Ouagadougou and Dori sites, respectively. Although the general decrease in Sahelian albedo between the dry and the wet seasons can be expected from biogeophysical considerations, recall that a relative uncertainty of at least 10% lies on the reference albedo estimates (Pinty et al., 1985; Pinty and Tanré, 1987).

The spatial and seasonal variations of the conversion factor F_{SOL} appear in Tables 2a and 2b. The spatial variations observed in the F_{SOL} factor between the three sites are mainly related to the spatial variations in the surface albedo values. Indeed, according to Stum et al. (1985) a decreasing albedo value leads to an increasing F_{SOL} factor. The large increase in water vapor which occurs between February and July explains the seasonal reduction in the F_{SOL} factor values; it is also responsible for the significant lowering of the double-way transmittances between these two days.

b. *Surface albedo maps*

Figures 1a and 1b show the surface albedo maps for 18 February and 2 July 1979 obtained with the ratio technique. All the albedo values are calculated with an hypothetical solar zenith angle equal to zero at each site. The black areas correspond to sites where the ratio technique is not applicable; in addition to the infrared radiances used for the identification of the cloudy areas, three criteria have been retained for deciding whether the technique can be applied or not: (i) a low value for the radiance standard deviation inside each site of 20 × 20 pixels to ensure that the spatially averaged radiances are representative of the site area; (ii) a good linear correlation between the diurnal radiances measured over neighboring sites; and (iii) a low value for the b_c term in (10) in order to limit the alteration of the results by possible large gradients in the optical properties of the actual atmosphere.

A great heterogeneity of surface albedo values is observed over the studied region; the values range from less than 0.20 at the southeastern part of the map to nearly 0.50 over the desert regions of Mali and Mauritania. Over the region located between latitudes 18°

TABLE 2b. As in Table 2a except on 2 July 1979.

Test sites	Time (UTC)	$T(\theta_0)_{a_T}$	$\frac{rd(\theta_0)\,a_{Td}}{a_T}$	F_{SOL}	ρ_0	$\rho(\theta_0, \theta_v, \psi)$	$a(\theta_0)$	$a(\theta_0 = 0)$
Ouagadougou	1200	0.531	0.178	2.604	0.177	0.222	0.220	0.220
Dori	1230	0.553	0.178	2.546	0.231	0.289	0.287	0.287
Fada-Ngourma	1200	0.566	0.178	2.599	0.180	0.225	0.223	0.223

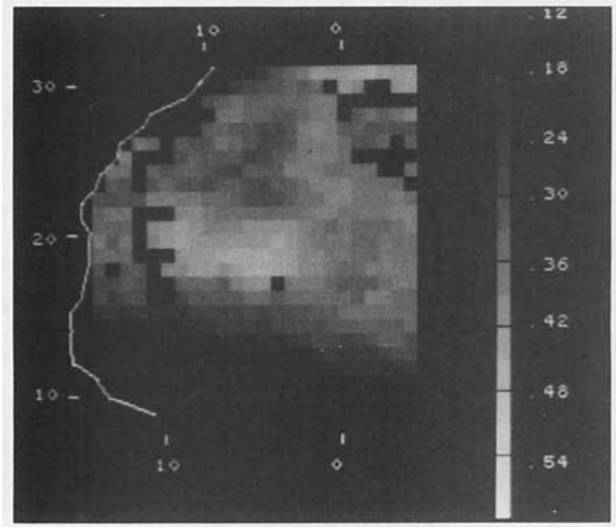

FIG. 1a. Surface albedo map for 18 February 1979.

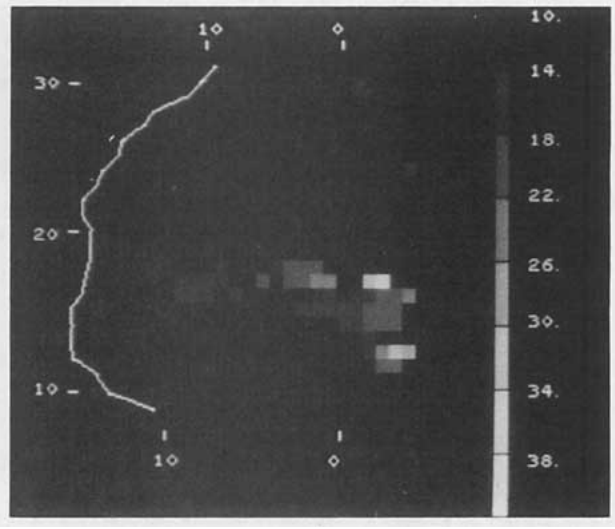

FIG. 2. Change (in percent) in surface albedo between 2 July and 18 February.

and 20°N and longitudes 2° and 10°W, the averaged albedo values are 0.440 ± 0.018 for 18 February and 0.458 ± 0.025 for 2 July 1979; over the same region Courel et al. (1984) have obtained values of 0.40–0.50 for the solar spectrum-weighted albedo from METEOSAT data and Rockwood and Cox (1978) have derived values greater than 0.42 from SMS data. A gradual increase of surface albedo with latitude clearly appears between 14° and 20°N. As previously discussed by Rockwood and Cox (1978), this variation is related to the different physical states of the surface. The major difference between the two maps lies in the important decrease of surface albedo values on 2 July, which is observed to the east of 5°N and south of 18°N; this feature can be linked to the northern migration of the ITCZ between the two months since the corresponding increase in atmospheric water amount leads to sensitive modifications of the surface state through biogeophysical mechanisms.

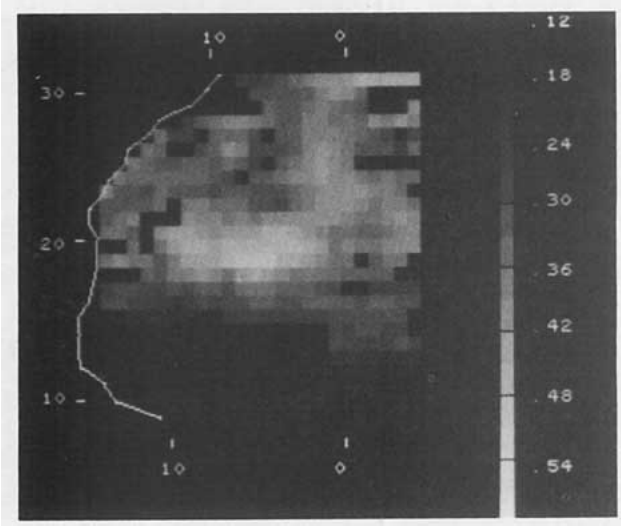

FIG. 1b. Surface albedo map for 2 July 1979.

Figure 2 represents the seasonal albedo change expressed through the SV index calculated with (11). All the SV values reported in this figure are negative and indicate a decrease in surface albedo between 18 February and 2 July. Some positive values (not shown) less than 10% have been found north of 20°N; these positive values are somewhat randomly located and can be interpreted in terms of uncertainty inherent to the ratio technique itself. On the contrary, the negative SV values with maximum near 40% constitute a consistent field of albedo change. The general patterns observed in surface albedo changes are somewhat different from those obtained by Pinty and Szejwach (1985) with the same data. The differences are mainly due to the fact that, in this previous study, the a_c term of (10) was not explicitly calculated and was given a value equal to 1. This assumption is acceptable as long as the ratio technique is applied over a region of limited spatial extension (~500 km). However, it can introduce significant errors when analyzing the seasonal albedo changes over a whole climatic region.

c. *Conversion factor*

According to section 4, the conversion factors F_{SOL} used to estimate broadband radiances have been simultaneously derived with the surface albedo values. As an example, the F_{SOL} maps obtained at 1130 UTC on 18 February and 2 July are given in Figs. 3a and 3b, respectively. From these maps, a variability of 10% can be observed over the studied region. Globally the higher F_{SOL} values are located over the lower surface albedo sites. The general lowering of the F_{SOL} factor on 2 July is explained by its angular dependency with

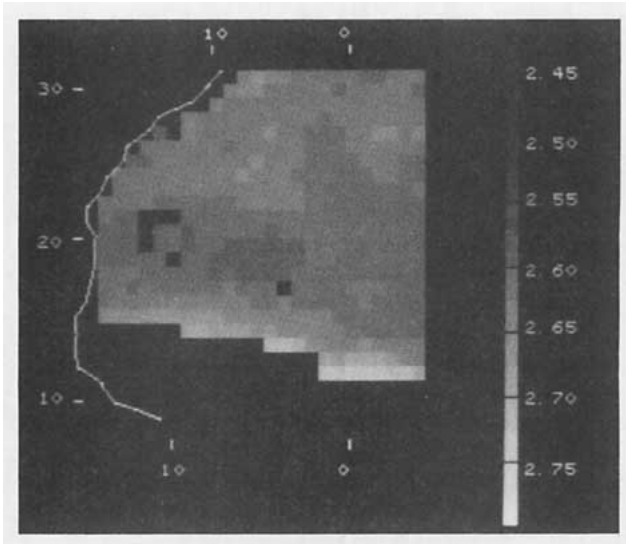

FIG. 3a. Conversion factor map for 18 February at 1130 UTC.

respect to the relative observational geometry. Obviously, with the changing angular conditions the observed F_{SOL} patterns undergo large modifications when considering other times of the day.

6. Discussion of the correction procedures

Starting from the METEOSAT filtered radiances for the retrieval of broadband surface albedos, the ratio technique includes correction procedures for the atmospheric effects, the spectral sampling by the sensor and the anisotropic properties of the surfaces. The importance and quality of the proposed corrections can be illustrated by the analysis of some relationships between planetary and surface albedos estimated with and without application of these corrections.

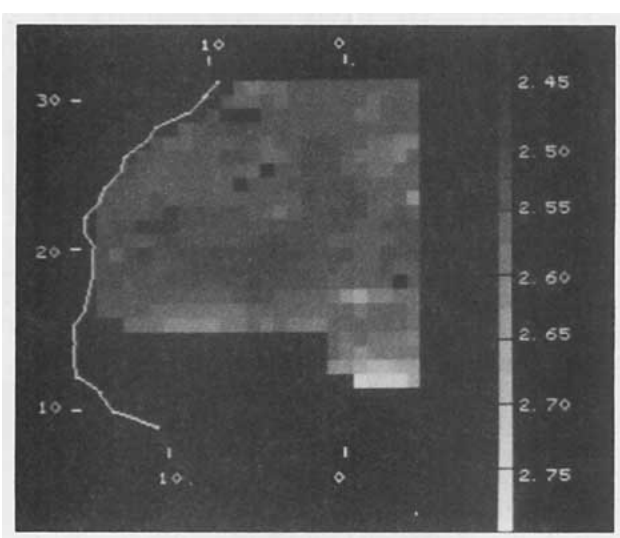

FIG. 3b. Conversion factor map for 2 July at 1130 UTC.

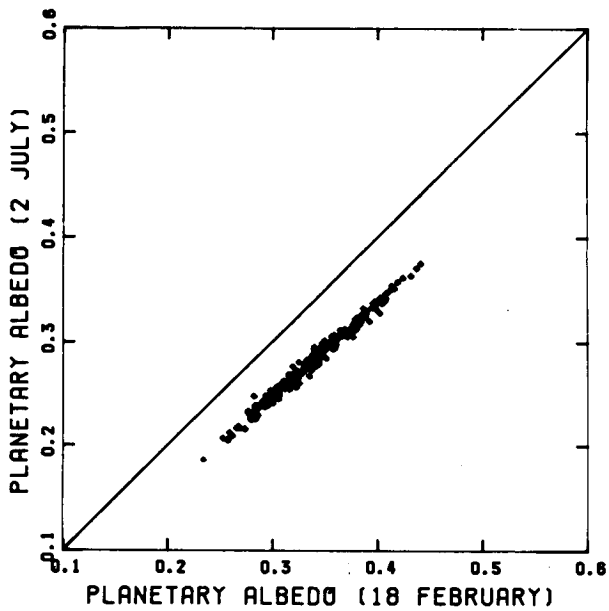

FIG. 4a. Planetary albedo for 2 July against planetary albedo for 18 February. For both days the values are calculated at 1130 UTC using (12).

a. *Atmospheric effects*

In order to appreciate the ability of the ratio technique to remove the masking effect due to the atmosphere, the relationship between the planetary albedos on 18 February and 2 July (Fig. 4a) can be compared to the one obtained for the corresponding surface albedos (Fig. 4b) over the desertic and semidesertic sites

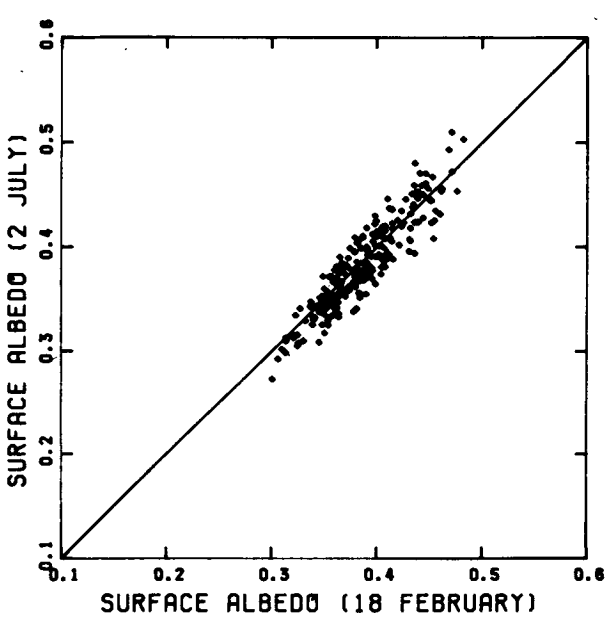

FIG. 4b. Surface albedo for 2 July against surface albedo for 18 February. For both days the values are calculated at 1130 UTC.

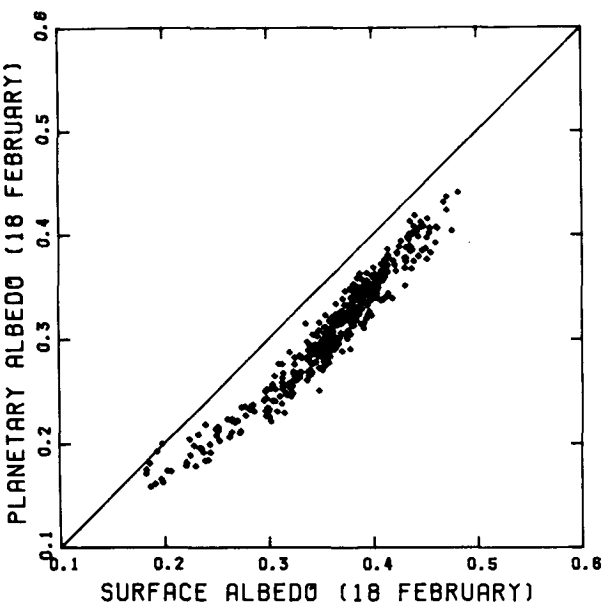

FIG. 5a. Relationship between planetary and surface albedo for 18 February at 1130 UTC.

located north of the latitude 17°N where no surface albedo change is expected (Eyre, 1968; Tucker, 1986). The planetary albedos $a^*(\theta_0)$ are calculated according to (12):

$$a^*(\theta_0) = \frac{\pi L_{SAT} F_{SOL}}{E_0 \cos(\theta_0) f(\theta_0, \theta_v, \psi)}, \tag{12}$$

where $f(\theta_0, \theta_v, \psi)$ is the anisotropic factor for the outgoing radiance at the top of the atmosphere.

In the present calculation of planetary albedos, the anisotropic factors have been derived from ERBE's data, and the bidirectional model proposed by Pinty and Ramond (1986) has been applied to achieve the angular interpolations. The planetary albedos reported in Fig. 4a are calculated with the actual angles of observation and illumination at 1130 UTC. Figure 4a clearly indicates that the optical atmospheric conditions are different between the two studied days. Indeed, the dependency of the planetary albedo with solar zenith angles less than 50° is sufficiently small to be neglected in the analysis of the relationship (see, for instance, Braslau and Dave, 1973). The relative lowering of the $a^*(\theta_0)$ values observed on 2 July signifies that the atmosphere is more absorptive to solar radiation than it was on 18 February. Note here that the change in the atmospheric conditions between the two days over the desertic and semidesertic regions is not well depicted by data taken from the scarce weather stations of the region. Since the corresponding surface albedo values are found to be approximately the same for the 2 days (Fig. 4b), we may conclude that the ratio technique provides a satisfactory procedure to remove the effects due to the atmosphere when estimating the surface albedo from remotely sensed observations.

The relationship between surface and planetary albedos on 18 February and 2 July are shown at 1130 UTC in Figs. 5a and 5b, respectively. The planetary and surface albedos are nearly identical when the surface albedo is slightly less than 0.2; when the surface albedo is greater than 0.2 the planetary albedo is always lower than the surface albedo. Presumably because of a higher absorptive atmosphere, this last feature is enhanced on 2 July. In Figs. 5a and 5b, the scattering of the points is also noticeable; although the errors inherent in the techniques we used for inferring the surface and the planetary albedos can contribute to this scattering, it is also likely to be assumed that the optical properties of the atmosphere vary over the whole climatic region.

b. Effects of the spectral response of the sensor

The correcting effects due to the conversion factors we used to derive broadband radiances from the METEOSAT radiances is illustrated in Fig. 6 in the case of 18 February at 1130 UTC. Assuming an isotropic radiation at the top of the atmosphere, Fig. 6 compares the broadband albedo a^*_{SOL} to the METEOSAT albedo a^*_{SAT} calculated as follows:

$$a^*_{SOL} = \frac{\pi L_{SAT} F_{SOL}}{E_0 \cos(\theta_0)} \tag{13}$$

$$a^*_{SAT} = \frac{\pi L_{SAT}}{E_{SAT} \cos(\theta_0)} \tag{14}$$

with

$$E_{SAT} = \int_{0.3}^{3\,\mu m} E_{0\lambda} \tau_{SAT\lambda} d\lambda.$$

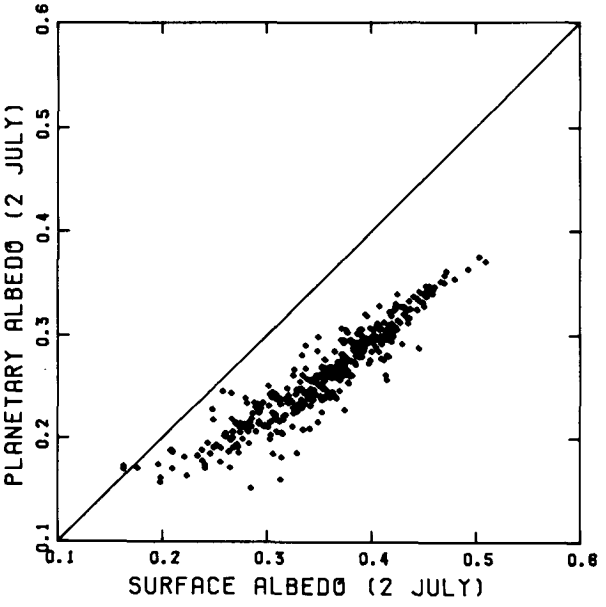

FIG. 5b. As in Fig. 5a except for 2 July.

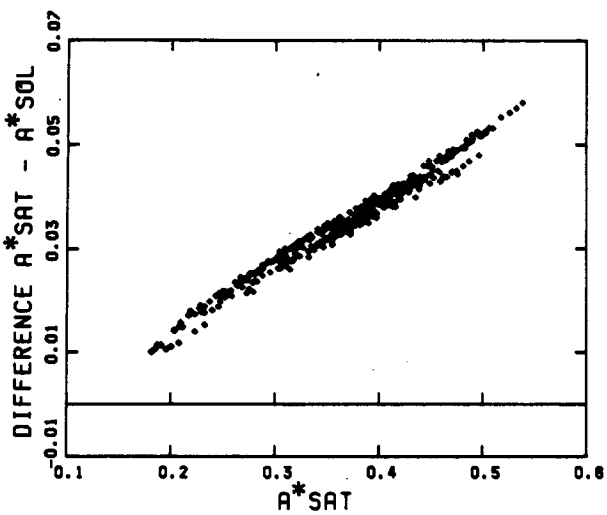

FIG. 6. Difference between METEOSAT and broadband planetary albedo against METEOSAT albedo. Values are for 18 February at 1130 UTC.

In Fig. 6, it is seen that the METEOSAT albedos are systematically greater than the corresponding broadband albedos; in the shown case the difference is about 10% of the mean value. This systematic overestimate, which is still greater in the 2 July case, is mainly due to the effects of atmospheric water vapor; indeed water vapor absorption occurs at wavelengths for which the METEOSAT visible channel has a spectral response which is low or null.

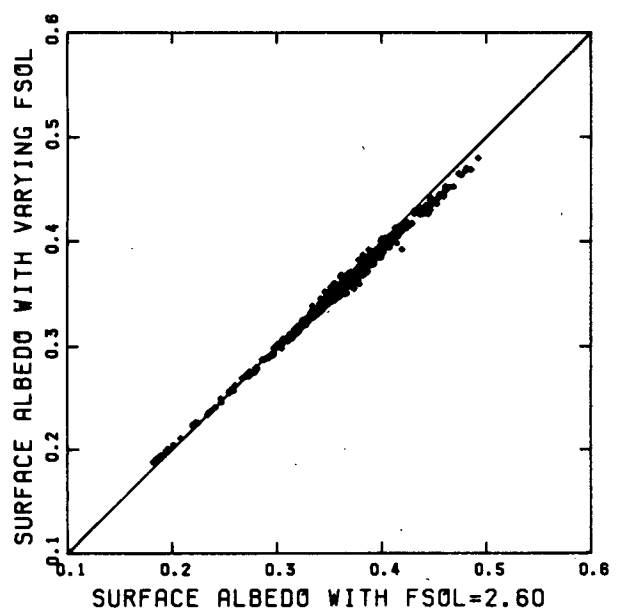

FIG. 7. Comparison of surface albedo estimated with the complete procedure for F_{SOL} calculation with surface albedo obtained with a mean F_{SOL} value equal to 2.60 and constant over the studied region. Values are for 2 July 1979.

In order to examine the sensitivity of the surface albedo results to F_{SOL} variations, the surface albedos obtained with a constant mean F_{SOL} value of 2.60 expectable from Koepke (1983) are compared in Fig. 7 to those obtained when applying the complete procedure for F_{SOL} calculation. The comparison shown for the 2 July case study is made by assuming that the surfaces behave like Lambertian surfaces [i.e., f_a/f_r equal to 1 in (7) and (10)]. To neglect the F_{SOL} variability yields a slight overestimate (underestimate) of the surface albedo for values greater than (less than) nearly 0.3. In the considered case, the differences reach approximately 5% of the surface albedo values; obviously with a higher (lower) mean F_{SOL} value, larger differences would be observed for the highest (lowest) albedo values.

c. *Anisotropy effects*

The correction factors, introduced to account for the anisotropic behavior of the surface as well as to assess planetary albedos from the outgoing radiances at the top of the atmosphere, exhibit intricate dependency on the relative geometry of illumination and observation. This intricacy is illustrated in Figs. 8a and 8b, where planetary albedos a^*_{SOL} calculated with (13) by assuming isotropic METEOSAT radiances are compared with planetary albedos $a^*(\theta_0)$ calculated with (12). Figures 8a and 8b, using METEOSAT data on 2 July, correspond to 1130 and 1500 UTC, respectively. At 1130 UTC, a^*_{SOL} is always greater than $a^*(\theta_0)$ so that the isotropic assumption leads to overestimated planetary albedos. On the contrary, at 1500 UTC $a^*(\theta_0)$ is greater than a^*_{SOL} and the largest relative departures between the two albedos are found over sites classified into the land region category. An example of the de-

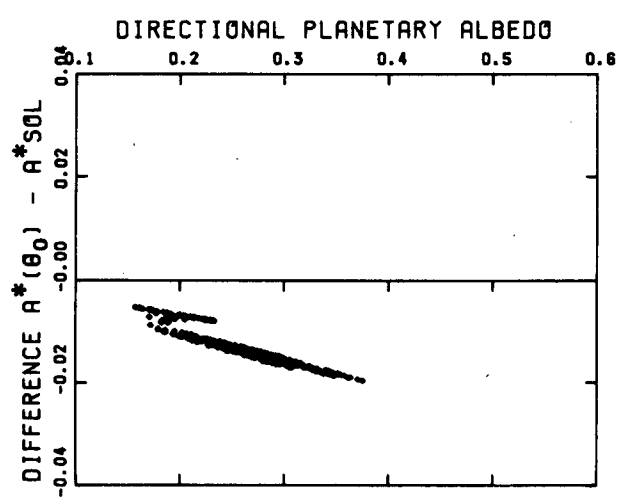

FIG. 8a. Difference between directional and Lambertian planetary albedo against the directional planetary albedo with METEOSAT radiance measurements. Values are for 2 July at 1130 UTC over the studied region.

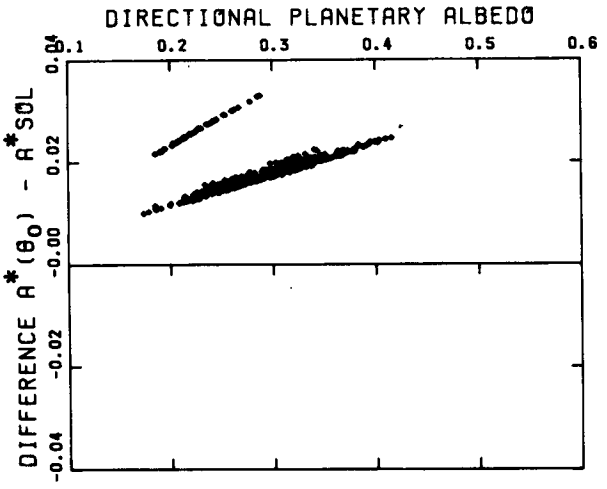

FIG. 8b. As in Fig. 8a except at 1500 UTC.

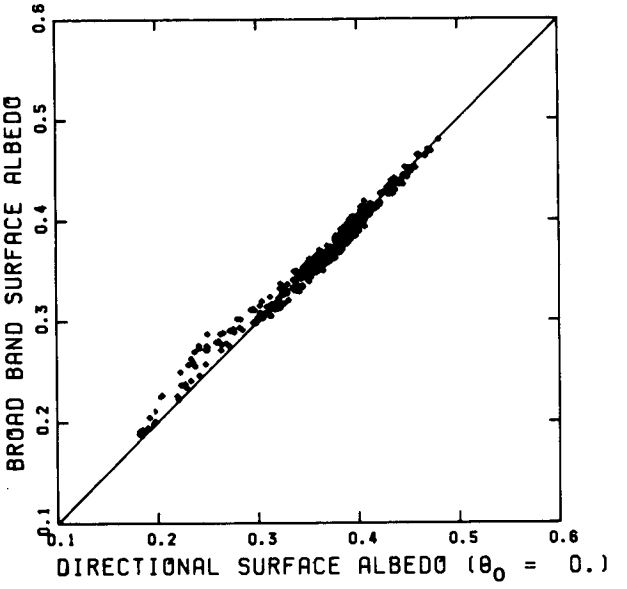

FIG. 10a. Comparison of directional surface albedo for an overhead sun with Lambertian surface albedo. Values are for 18 February.

pendency of the observed planetary albedos a^*_{SOL} and $a^*(\theta_0)$ with respect to solar zenith angle is given in Fig. 9 together with a theoretical curve deduced from results given by Koepke and Kriebel (1987) for a clear air atmosphere. The observations presented in Fig. 9 concerned a site located between 20°–19°N and 0°–1°E, and are taken from 1030 to 1500 UTC on 18 February. The theoretical curve has been obtained by using the directional surface albedos derived from the ratio technique over the considered site. Figure 9 emphasizes the major difference in a^*_{SOL} and $a^*(\theta_0)$ since with an increasing solar zenith angle, a^*_{SOL} tends to decrease whereas $a^*(\theta_0)$ tends to increase. The comparison between $a^*(\theta_0)$ variations and the theoretical curve leads to the conclusion that correction by the anistropic factor yields a more physically realistic result about the directional properties of the estimated planetary albedo.

However, the anisotropic properties of the surfaces which are mainly responsible for the angular dependency of the satellite radiances seem to be rubbed out by the ratio technique in our case studies. Indeed, Figs. 10a and 10b obtained on 18 February and 2 July, respectively, show a reasonably good agreement between the surface albedos calculated for overhead sun con-

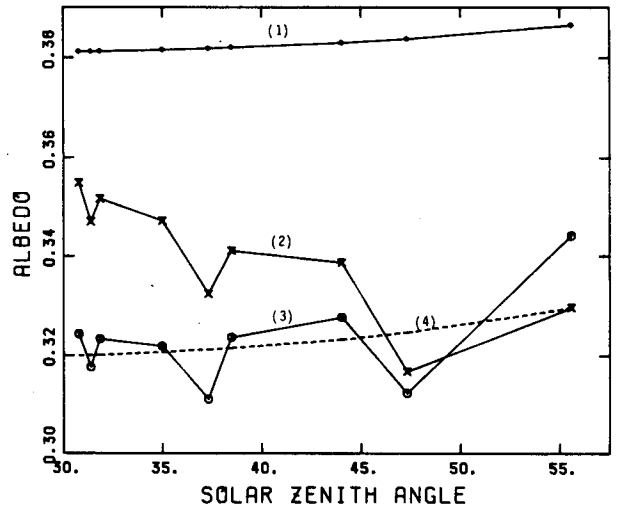

FIG. 9. Variations with solar zenith angle of 1) surface albedo; 2) Lambertian planetary albedo a^*_{SOL}; 3) directional planetary albedo $a^*(\theta_0)$; 4) theoretical planetary albedo for a clear air atmosphere. Values are for 18 February from 1030 to 1500 UTC over a site located at 19°–20°N, 0°–1°E.

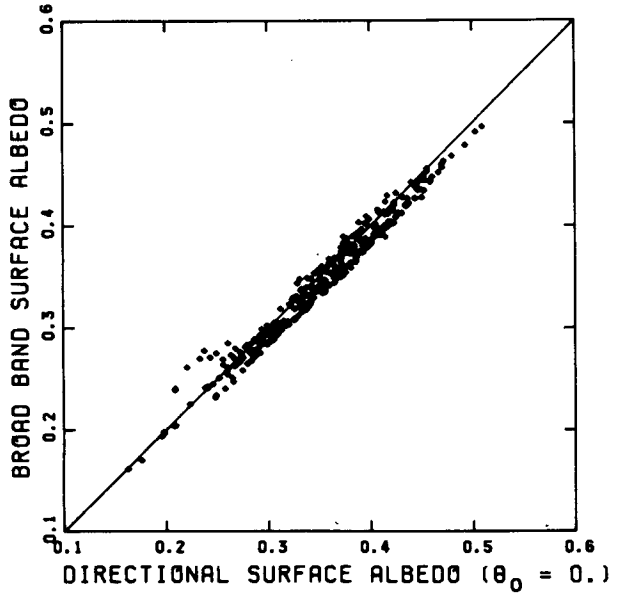

FIG. 10b. As in Fig. 10a except for 2 July.

ditions and the surface albedos estimated with the ratio technique by assuming that the surfaces possess Lambertian properties. For both study cases, the largest discrepancies between the two albedo estimates are observed over sites which belong to the land category; although the differences are not large, it can be noticed on 2 July that the albedos over desert sites tend to be underestimated when using the Lambertian assumption.

7. Summary and concluding remarks

The method developed in this paper is devoted to the quantitative estimate of surface reflection properties from geostationary satellite data. The diurnal sampling of the outgoing radiance at the top of the atmosphere and a surface radiation measurement in the application area are both required for the removal of the masking effect due to the atmosphere. The proposed method includes spectral and angular correction procedures in order to infer broadband directional albedos from the filtered radiances measured in the viewing direction of the geostationary satellite.

Application of the method with METEOSAT observations allowed albedo maps to be derived on 18 February and 2 July 1979 over western Africa. An extensive range (0.20 to 0.50) of surface albedo values has been found over this region. The comparison of the two maps has shown the well-known surface albedo decrease over the Sahel with the onset of the wet season and the consistent albedo values estimated over the desert regions. This latter result is important for the validation of the method since it has been obtained for two cases where the atmospheric and the angular conditions are significantly different. In future applications of the ratio technique over western Africa, it is possible to use as reference sites the desert areas where no albedo changes are observed.

The analysis of the relationships between surface and planetary albedos has demonstrated the need for correction procedures in order to get realistic relationships between these two quantities. It is an interesting outcome of the proposed method to allow the analysis of such relationships which contain information about the shortwave atmospheric budget. From this point of view, our approach differs in a basic way from commonly used techniques (see, e.g., Preuss and Geleyn, 1980; Chen and Ohring, 1984) which assume the a priori knowledge of atmospheric conditions and where the derivation of surface albedo is achieved with the help of atmospheric coefficients deduced from simulation studies of the planetary albedo.

Several data sources are involved in the application of the method in order to get the auxiliary information which is essential in a remote sensing approach. In our case study, the required information has been taken from multispectral Tiros-N satellite data, Nimbus-7 anisotropic factors, surface meteorological networks and also some climatological data. Note that these data often yield an approximate description or value of the needed parameter (conversion factors, anisotropic factors, . . .). These data allow the description on a global scale of the major existing features concerning the optical state of the surface and of the atmosphere.

With regard to the scale and precision recommended by climate modelers in surface albedo estimates, the method appears to be relevant for climatological analyses. Our study has been conducted over western Africa. However, since the required data can be routinely derived on a global basis, the method can be used over other climatic regions viewed by geostationary satellites.

Acknowledgments. We thank Dr. Koepke for fruitful and informative discussion on this topic. The authors are indebted to Mr. J. Stum and Dr. Y. Pointin for helpful comments and suggestions about the manuscript. Computer programming support provided by R. Pejoux is deeply appreciated. The efforts of Mrs. C. Paquet, O. Guillot and J. Squarise in preparing the manuscript are gratefully acknowledged.

APPENDIX

Estimate of the a_{Td} Factor

According to (6), knowledge of the diffuse radiation incident at the surface is required in the satellite equation for the retrieval of the bidirectional and the hemispherical reflectances of the surface. In order to use ground based measurements of the diffuse radiation as an input parameter in the radiance equation, one has to estimate the extinction of this signal by the atmosphere along the viewing direction of the satellite. This estimate can be achieved with the help of the factor a_{Td} defined as follows:

$$a_{Td}=\frac{T_E(\theta_0,\theta_v)}{E(\theta_0)}, \tag{A1}$$

where $E(\theta_0)$ is the diffuse transmittance incident at the surface and $T_E(\theta_0, \theta_v)$ is the corresponding transmittance at the satellite level.

Following the computational method suggested by Pinty and Tanré (1987) when studying the a_T factor, the 5S code (Simulation of the Satellite Signal in the Solar Spectrum) developed by Tanré et al. (1986) can be used to calculate $T_E(\theta_0, \theta_v)$ and $E(\theta_0)$ for a variety of cases corresponding to clear sky conditions. According to the 5S code algorithm, $T_E(\theta_0, \theta_v)$ and $E(\theta_0)$ are computed from:

$$T_E(\theta_0,\theta_v)=\frac{\int_{0.3}^{3\ \mu m} E_{0\lambda}\cos(\theta_0)\,\widehat{tg}_{\lambda}(\theta_0,\theta_v)E_{d\lambda}(\theta_0)T_{\lambda}(\theta_v)\alpha_{\lambda}d\lambda}{\int_{0.3}^{3\ \mu m} E_{0\lambda}\cos(\theta_0)\alpha_{\lambda}d\lambda} \tag{A2}$$

$$E(\theta_0) = \frac{\int_{0.3}^{3\ \mu m} E_{0\lambda} \cos(\theta_0)\, \widehat{tg}_{\lambda}(\theta_0) E_{d\lambda}(\theta_0) d\lambda}{\int_{0.3}^{3\ \mu m} E_{0\lambda} \cos(\theta_0) d\lambda}, \quad \text{(A3)}$$

where θ_0 and θ_v are the solar zenith angle and the satellite viewing angle, respectively; E_0 is the solar irradiance; α the surface reflectance; $\widehat{tg}(\theta_0, \theta_v)$ the total transmission factor for the effective gaseous absorption along the optical path from the sun to the satellite via the surface; $E_d(\theta_0)$ the diffuse downward transmission factor of the scattering atmosphere; $T(\theta_v)$ the total (direct + diffuse) upward transmission factor of the scattering atmosphere along the viewing direction of the satellite.

The details of the calculation of the intervening transmission factors are given in Tanré et al. (1986). The dependency of the surface albedo with wavelength is schematically described by the spectral band ratio analogous to the vegetation index available from AVHRR data.

Table A1 lists the dataset we used in the computation for the eight explicit variables. From the sample we considered here, it appears that, for a given satellite angle, the spectral band ratio, the visibility and the water vapor content are the most sensitive variables leading to significant changes in the a_{Td} factor. The major change in the a_{Td} factor is due to the variations of the spectral band ratio; when the spectral band ratio increases, a large decreasing rate of the a_{Td} factor is observed. This behavior is due to the fact that, when the spectral band ratio takes high values, part of the diffuse radiation is reflected at wavelengths where water vapor absorption is important.

Using a polynomial expansion, the following parameterized expression has been established for the a_{Td} factor:

$$a_{Td} = 0.7574 + f_1(I - 0.2) + f_2(\text{VIS} - 19) + f_3(U_{H_2O} - 3) + f_4(\theta_v - 15). \quad \text{(A4)}$$

TABLE A1. Values taken by the input variables in the computation of the factor a_{Td}. Here ψ is the relative azimuth angle; VIS the horizontal visibility; U_{H_2O} the water vapor content; U_{O_3} the total ozone amount and I the spectral band ratio. The values in parentheses indicate the $\delta_{.55\ \mu m}$ aerosol optical depth corresponding to the visibility values.

Variable	Value			
θ_0 (deg)	0	15	30	
θ_v (deg)	0	15	30	
ψ (deg)	0	90	180	
VIS (km)	35	19	11	(0.1, 0.3, 0.5)
U_{H_2O} (cm)	1	3	5	
U_{O_3} (cm atm)	0.20	0.25	0.30	
α	0.2	0.3	0.4	
I	0	0.2	0.4	0.6

TABLE A2. Order and coefficients of polynomial expressions f_j appearing in (A4).

Variable (x_j)	Order no. of $f_j(x_j) = a_i x_j^i$	Coefficients (a_i)	Exponent (i)
$I - 0.2$	2	0.6999 $E-01$	2
		−0.4741 $E-0$	1
VIS − 19	2	−0.9948 $E-04$	2
		0.1754 $E-02$	1
$U_{H_2O} - 3$	2	0.1187 $E-0$	2
		−0.2475 $E-02$	1
$\theta_v - 15$	2	−0.2578 $E-04$	2
		−0.7200 $E-03$	1

In this expression, only the most sensitive variables are retained: I denotes the spectral band ratio, VIS the horizontal visibility in kilometers and U_{H_2O} the total water vapor content. The polynomials f_j are given in Table A2. The medium 0.7574 value is obtained for the following model conditions: $I = 0.2$, VIS = 19 km, $U_{H_2O} = 3$ cm, $U_{O_3} = 0.25$ cm atm, $\theta_0 = 15°$, $\theta_v = 15°$, $\psi = 180°$, and $\alpha = 0.3$.

The use of (A4) is confined by the choice we made to describe the surface and the atmospheric optical states through global and routinely measured variables; as a consequence, this parameterized expression is suitable for global approaches but it may be irrelevant for more specific surface and atmospheric conditions.

REFERENCES

Berkofsky, L., 1976: The effect of variable surface albedo on the atmospheric circulation in desert regions. *J. Appl. Meteor.*, **15**, 1139–1144.

Bouka Biona, C., and C. Boutin, 1985: Evolution saisonnière de l'échelle spatiale du rayonnement solaire global en zone sahélienne. *Atmos. Ocean*, **23**, 67–79.

Braslau, N., and J. V. Dave, 1973: Effect of aerosols on the transfer of solar energy through realistic model atmospheres. Part I: Non-absorbing aerosols. *J. Appl. Meteor.*, **12**, 601–615.

Charney, J. G., 1975: Dynamics of deserts and drought in the Sahel. *Quart. J. Roy. Meteor. Soc.*, **101**, 193–202.

——, W. J. Quirk, S-H Chow and J. Kornfield, 1977: A comparative study of the effects of albedo change on drought in semi-arid regions. *J. Atmos. Sci.*, **34**, 1366–1385.

Chen, T. S., and G. Ohring, 1984: On the relationship between clear-sky planetary and surface albedos. *J. Atmos. Sci.*, **41**, 156–158.

Courel, M. F., R. S. Kandel and S. I. Rasool, 1984: Surface albedo and the Sahel drought. *Nature*, **307**, 528–531.

Deschamps, P. Y., M. Herman and D. Tanré, 1981: Influence de l'atmosphère en télédétection des ressources terrestres. Modélisation et possibilités de corrections. Spectral Signatures of Objects in Remote Sensing, INRA, Avignon, France, 543–558.

Eyre, S. R., 1968: Vegetation and soils. A world picture. Arnold, 328 pp.

Hapke, B. W., 1963: A theoretical photometric function for the lunar surface. *J. Geophys. Res.*, **68**, 4571–4586.

Henderson-Sellers, A., and M. F. Wilson, 1983: Surface albedo data for climatic modeling. *Rev. Geophys. Space Phys.*, **21**, 1743–1778.

Justus, C. G., and M. V. Paris, 1985: A model for solar spectral irradiance and radiance at the bottom and top of a cloudless atmosphere. *J. Climate Appl. Meteor.*, **24**, 193–205.

Kieffer, H. H., T. Z. Martin, A. R. Peterfreund and B. M. Jakosky,

1977: Thermal and albedo mapping of Mars during the Viking primary mission. *J. Geophys. Res.*, **82,** 4249–4291.

Koepke, P., 1982: Vicarious satellite calibration in the solar spectral range by means of calculated radiances and its application to METEOSAT. *Appl. Opt.*, **21,** 2845–2854.

——, 1983: Calibration of the VIS-Channel of METEOSAT 2. *Adv. Space Res.*, **2,** 93–96.

——, and K. T. Kriebel, 1987: Improvement of the shortwave cloud-free radiation budget accuracy. Part I: Numerical achievement including surface anisotropy. *J. Climate Appl. Meteor.*, **26,** 374–395.

Minnaert, M., 1941: The reciprocity principle in lunear photometry. *Astrophys. J.*, **93,** 403–410.

Otterman, J., 1974: Baring high-albedo soils by overgrazing: Hypothesised desertification mechanism. *Science,* **186,** 530–533.

Pinty, B., and G. Szejwach, 1985: A new technique for inferring surface albedo from satellite observations. *J. Climate Appl. Meteor.*, **24,** 741–750.

——, and D. Ramond, 1986: A simple bidirectional reflectance model for terrestrial surfaces. *J. Geophys. Res.*, **91,** 7803–7808.

——, and D. Tanré, 1987: The relationship between incident and double-way transmittances: An application for the estimate of surface albedo from satellite over the African Sahel. *J. Climate Appl. Meteor.*, **26,** 892–896.

——, G. Szejwach and J. Stum, 1985: Surface albedo over the Sahel from METEOSAT radiances. *J. Climate Appl. Meteor.*, **24,** 108–113.

Preuss, H., and J. F. Geleyn, 1980: Surface albedoes derived from satellite data and their impact on forecast models. *Arch. Meteor. Geophys. Bioklim., Ser. B,* **29,** 345–356.

Reitan, C. H., 1963: Surface dew point and water vapor aloft. *J. Appl. Meteor.*, **2,** 776–779.

Rockwood, A. A., and S. K. Cox, 1978: Satellite inferred surface albedo over Northwestern Africa. *J. Atmos. Sci.*, **35,** 513–522.

Stum, J., B. Pinty and D. Ramond, 1985: A parameterization of broadband conversion factors for METEOSAT visible radiances. *J. Climate Appl. Meteor.*, **24,** 1377–1382.

Sud, Y. C., and M. Fenessy, 1982: A study of the influence of surface albedo on July circulation in semi-arid regions using GLAS GCM. *J. Climatol.*, **2,** 105–125.

Tanré, D., C. Deroo, P. Duhaut, M. Herman, J. J. Morcrette, J. Perbos and P. Y. Deschamps, 1986: Simulation of the Satellite Signal in the Solar Spectrum (5 S), User's Guide. Laboratoire d'Optique Atmosphérique, U.S.T.L., 59655 Villeneuve d'Ascq Cédex, France, 341 pp.

Tarpley, J. D., S. R. Schneider and R. L. Money, 1984: Global vegetation indices from the NOAA-7 meteorological satellite. *J. Climate Appl. Meteor.*, **23,** 491–494.

Taylor, V. R., and L. L. Stowe, 1984: Reflectance characteristics of uniform earth and cloud surfaces derived from Nimbus-7 ERB. *J. Geophys. Res.*, **89,** 4987–4996.

Tucker, C. J., 1986: Maximum normalized difference vegetation index images for sub-Saharan Africa for 1983–1985. *Int. J. Remote Sens.*, **7,** 1383–1384.